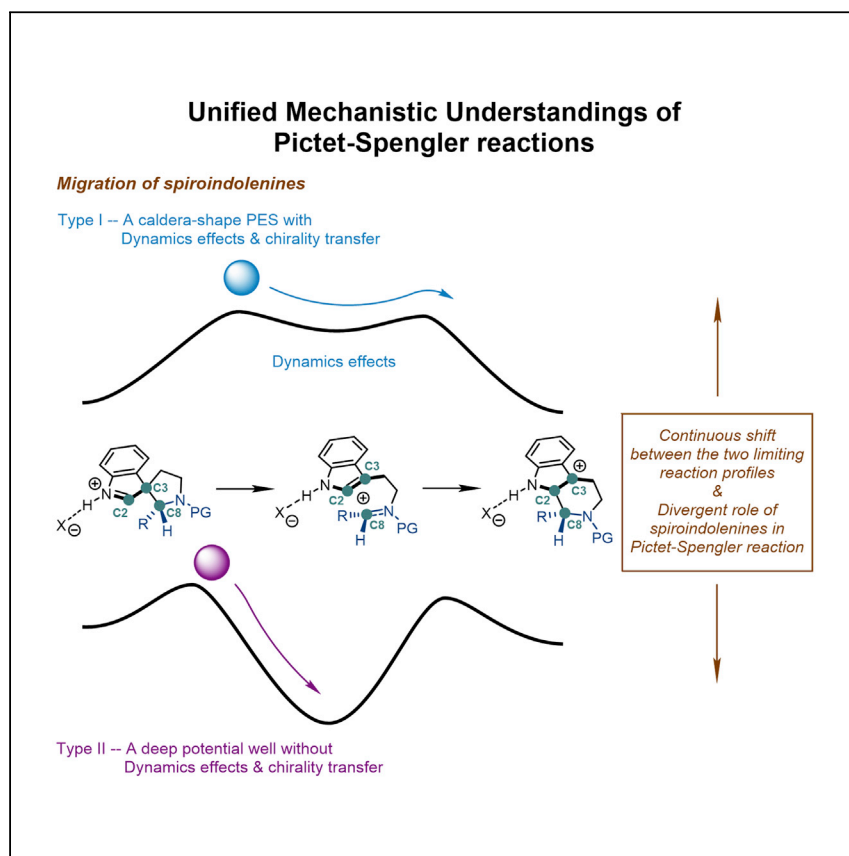


## Article

## Unified Mechanistic Understandings of Pictet-Spengler Reactions



Chao Zheng, Zi-Lei Xia, Shu-Li You

zhengchao@sioc.ac.cn (C.Z.)  
slyou@sioc.ac.cn (S.-L.Y.)

**HIGHLIGHTS**

Dynamics effects might be involved in Pictet-Spengler reactions

Spiroindolenine can be either a productive or a non-productive intermediate

DFT calculations and direct molecular dynamics simulations have been utilized

Pictet-Spengler reactions have widely been employed in the synthesis of polycyclic-indole-derived natural products. However, the mechanism of this reaction has remained as a controversial research topic. In this article, You and co-workers performed combined density functional theory calculations and direct molecular dynamics simulations to provide unified mechanistic understandings of Pictet-Spengler reactions with an emphasis on the divergent role played by spiroindolenine intermediates. The key theoretical predictions are well supported by further experiments.



Article

# Unified Mechanistic Understandings of Pictet-Spengler Reactions

Chao Zheng,<sup>1,\*</sup> Zi-Lei Xia,<sup>1</sup> and Shu-Li You<sup>1,2,\*</sup>

## SUMMARY

Pictet-Spengler reactions are extensively utilized in the synthesis of various indole alkaloids. However, their mechanisms have been a controversial research topic. The role of spiroindolene, the generally proposed key intermediate in catalytic asymmetric Pictet-Spengler reactions, remains elusive. Herein, combined density functional theory calculations and direct molecular dynamics simulations reveal that the role of this intermediate is divergent. The spiroindolene acts as either a productive or a non-productive intermediate depending on the shape of the potential energy surface. In the former case, dynamic effects play an important role in the rearrangement of spiroindolene, which can occur without passing through the intervening transition states along the reaction coordinates. In the latter case, the formation of spiroindolene is only an off-cycle equilibrium. These theoretical predictions were verified experimentally. Furthermore, these insights were applied to seven reported catalytic asymmetric Pictet-Spengler reactions, leading to unified mechanistic understandings of this synthetically enabling reaction.

## INTRODUCTION

Capturing and characterizing reactive intermediates in homogeneous catalytic reactions undoubtedly holds a significant position in modern organic chemistry, since it can provide first-hand information about the details of the reaction mechanism. Thanks to the exponentially increasing computational capability and constantly emerging novel theoretical methods, computational chemistry has evolved as a powerful tool for mechanistic studies.<sup>1–4</sup> It is complementary to the direct isolation of reactive intermediates or the *in situ* observation of them by sophisticated spectroscopies, and especially useful when those intermediates are too unstable to be isolated or their lifetimes are considerably shorter than the timescales of the spectroscopic methods. Conventionally, density functional theory (DFT) calculations are widely employed to reveal informative structural and energetic properties of key transition states and intermediates. Notably in recent years, direct molecular dynamics simulations<sup>5–11</sup> have found broad applications in interpreting unusual profiles of organic reactions whose product distribution and stereochemistry are determined by the shape of the potential energy surface (PES) or non-statistical dynamics effects, rather than by the relative heights of energetic barriers, and therefore cannot be well described by classic transition state theory (TST).<sup>12–29</sup>

Pictet-Spengler reactions are among the most extensively utilized methods in the synthesis of various indole alkaloids.<sup>30–34</sup> Moreover, their mechanistic aspect is intriguing and has been a topic of intensive research for quite a long time.<sup>35–42</sup> In general, two reaction paths are proposed (**Scheme 1**): the initial iminium ion I generated from the condensation between the corresponding tryptamine and aldehyde might

## The Bigger Picture

The unique charm of synthetic chemistry stems from its room for creativity in breaking and constructing chemical bonds. Developing novel synthetic methodologies is the central task of fundamental organic chemistry, which can facilitate or enable access to valuable classes of compounds or materials. The Pictet-Spengler reaction is a key method for the synthesis of indole-derived natural products, an important class of compounds in drug discovery. Rational design of new chemical reactivity largely relies on deep mechanistic understandings. However, because of the inherent complexity of systems on the molecular level, usually a reaction mechanism can be perturbed by subtle changes of single reaction parameters. Hence, pursuing unified mechanistic understandings of synthetically enabling reactions is of great significance academically and can pave the way for crucial industrial synthetic applications in various fields.

cyclize directly at the C2 position of the indole ring, delivering protonated tetrahydro- $\beta$ -carboline II (path a). Alternatively, I might first undergo spiroindolization, giving five-membered-ring aza-spiroindolenine III (step 1, path b), then the migration of the iminium moiety yielding the same intermediate II (step 2, path b). From intermediate II, no matter by which reaction path it is generated, a proton abstraction process delivers final Pictet-Spengler product IV. A key issue that still remains elusive is the role played by intermediate III herein. Although it is well known that related spiroindolenine compounds can be synthesized independently,<sup>43</sup> to the best of our knowledge direct evidence supporting the validity of path b under catalytic asymmetric Pictet-Spengler conditions is not available. Therefore, providing a thorough and unified mechanistic picture of Pictet-Spengler reactions is of great importance.

In the past few years, we have looked into the mechanism of Pictet-Spengler-type reactions with Ir-catalyzed asymmetric allylic dearomatization reaction as a probe (**Scheme 2**).<sup>44–51</sup> On the basis of our mechanistic understandings, we have synthesized a series of enantioenriched five-membered-ring carbo- and aza-spiroindolenines, and have shown the possibility that their stereoselective migration can be achieved in a highly controllable fashion. DFT calculations (PBE1PBE/6-311+G\*\*) demonstrated that the close interaction between the electron-rich indole ring and the positively charged migratory group is critical for the chirality maintenance during the migration process.<sup>52</sup> However, a major drawback of these studies is that they did not prove the necessity of the involvement of the five-membered-ring aza-spiroindolenine intermediates as well as their stereoselective migration in real Pictet-Spengler reactions. To address this issue, we recently performed combined DFT calculations and direct molecular dynamics simulations of Pictet-Spengler reactions and revealed that the formation of spiroindolenine intermediate can be a kinetically competitive pathway compared with the direct C2 cyclization. The roles played by spiroindolenine intermediates are highly dependent on the shape of the PES. In particular, significant dynamics effects are observed for the prototype substrate having an electron-withdrawing group on the iminium nitrogen. In this case, spiroindolenine acts as a productive intermediate and its stereochemical information can be transferred to the final product very effectively. On the other hand, in the reaction of the prototype substrate with an electron-donating group on the iminium nitrogen, the formation of spiroindolenine is only an off-cycle equilibrium. The theoretical predictions were further supported experimentally. On the basis of these results, unified mechanistic understandings of Pictet-Spengler reactions were postulated. Herein, we report the details of this study.

## RESULTS

### DFT Calculations on the Prototype Pictet-Spengler Reactions

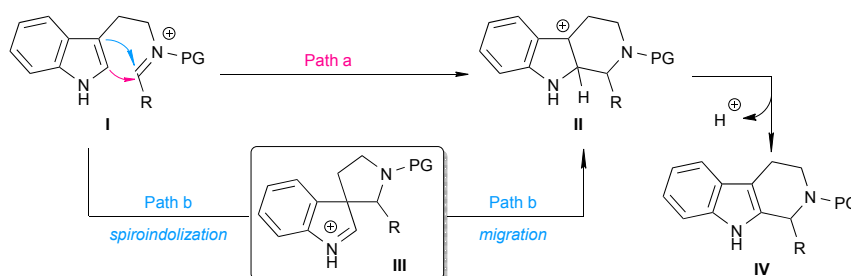
In this study, toslyc acid-catalyzed Pictet-Spengler reactions of two prototype substrates containing either a N-Bn (series A) or a N-Tf (series B) iminium moiety were first investigated by DFT calculations at the PBE1PBE/6-311+G\*\* level of theory (**Figure 1**). In both cases, the reaction starts from an *E*-iminium precursor (I-A, 0.0 kcal/mol; or I-B, 0.0 kcal/mol) generated from the condensation between the corresponding tryptamine and an aldehyde. Structurally, I-A and I-B are quite different from each other in terms of the distances between their corresponding iminium moiety and the indole ring (defined as  $I = \frac{1}{2} [B(C2-C8) + B(C3-C8)]$ ) (**Figure 2**). A small  $I$  value of about 2.5 Å in I-B indicates some interactions between the positively charged N-Tf iminium moiety and the electron-rich indole ring of this species. Atoms in molecules (AIM) topological analysis<sup>53</sup> revealed the existence of bond path and bond critical point between these two moieties. Wiberg bond indices<sup>54</sup>

<sup>1</sup>State Key Laboratory of Organometallic Chemistry, Center for Excellence in Molecular Synthesis, Shanghai Institute of Organic Chemistry, University of Chinese Academy of Sciences, Chinese Academy of Sciences, 345 Lingling Lu, Shanghai 200032, China

<sup>2</sup>Lead Contact

\*Correspondence: zhengchao@sioe.ac.cn (C.Z.), slyou@sioe.ac.cn (S.-LY.)

<https://doi.org/10.1016/j.chempr.2018.06.006>



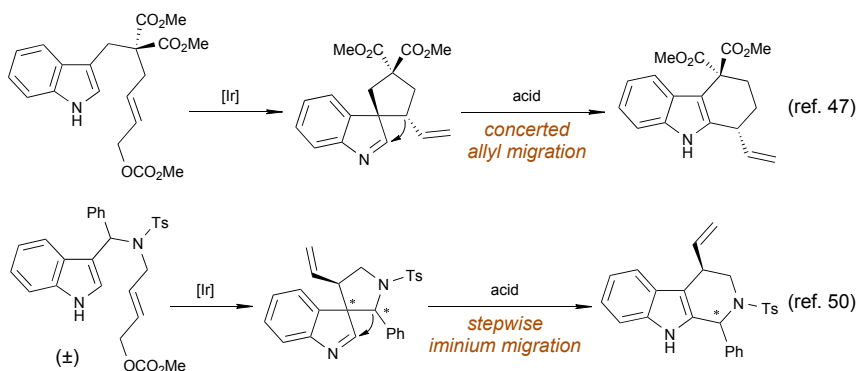
Scheme 1. General Mechanistic Proposal of Pictet-Spengler Reaction

between C2 and C8 (0.19) and C3 and C8 (0.16) also confirm some weak bonding interaction between these atom pairs. On the other hand, A large *l* value of about 3.2 Å was observed in I-A. Accordingly, the interaction between the N-Bn iminium moiety and the indole ring can be safely ignored.

The energetic barriers of nucleophilic attacks at the C2 or C3 positions of the indole ring (TS1 and TS2) are of undoubtedly importance in understanding the mechanism of Pictet-Spengler reactions. We employed two parameters, *d* (the energy difference between TS1 and TS2, defined as  $d = \Delta G(\text{TS2}) - \Delta G(\text{TS1})$ ) and *h* (the average barrier height of TS1 and TS2, defined as  $h = \frac{1}{2}[\Delta G(\text{TS1}) + \Delta G(\text{TS2})]$ ), to characterize these nucleophilic attacks. In both cases, the nucleophilic attacks at the C2 or C3 positions are almost equally accessible. A small or even negligible *d* value was observed for series A ( $d_A = 1.2$  kcal/mol) and B ( $d_B = 0.0$  kcal/mol), respectively, which indicates that the formation of spiroindolenines (III-A, 3.5 kcal/mol and III-B, -17.5 kcal/mol) is a kinetically competitive pathway compared with direct C2 cyclization in their corresponding reactions. However, the average barrier heights of the two transition states are rather different. Considerable energetic barriers should be overcome for both spiroindolization and C2 cyclization in series A ( $h_A = 13.5$  kcal/mol), whereas such barriers are very small in series B ( $h_B = 0.4$  kcal/mol). Notably, benchmark calculations on *d* and *h* values with various density functionals, including M06-2X, ωB97X-D, and B3LYP-D3(BJ), gave qualitatively consistent results (see Tables S1 and S2 for details). It should be noted that the differences between the two systems in terms of general energetics of the spiroindolization and C2 cyclization processes, as well as structural parameters of iminium precursors, will result in significantly varied mechanistic scenarios, especially regarding whether or not dynamics effects play a role in the migration of spiroindolene intermediate (vide infra).

Although both III-A and III-B can be formed effectively, neither of them is the global minimum of the corresponding PES. In fact, direct C2 cyclization leads to protonated tetrahydro-β-carbolines II-A (9.4 kcal/mol) and II-B (-12.0 kcal/mol), from which the irreversible proton abstraction by tosylate anion (TS3-A, 15.7 kcal/mol; TS3-B, -10.6 kcal/mol) furnishes tetrahydro-β-carboline as the thermodynamically most stable species in each system (IV-A, -4.2 kcal/mol; IV-B, -27.7 kcal/mol). Notably, the deprotonation is the rate-determining step in series A,<sup>39,41</sup> whereas on the other hand it is kinetically trivial in series B.

Given that III-A and III-B can be afforded effectively and at the same time are not the thermodynamically most stable species in each series, their downstream transformations become quite intriguing. This is also the most elusive part of the mechanistic puzzle of Pictet-Spengler reactions. On the basis of the knowledge of *d* and *h* values in both systems, we envisioned that the downstream transformations of III-A or III-B should be



**Scheme 2. The Synthesis and Migration of Spiroindolenines**

highly dependent on the shape of the corresponding PES. A better description of this issue comes from the calculated two-dimensional PESs of the two series (electronic energies at the PBE1PBE/6-31G\*\* level of theory) with respect to the distances of C2–C8 and C3–C8 bonds (Figure 3). First, the retro-process of the spiroindolization in series A was considered (Figure 3A). A particle coming from III-A via TS2-A (2.53, 2.02) will most likely be trapped in the deep potential well around local minimum I-A (3.22, 3.21), which indicates that the direct transformation from III-A to II-A might be interrupted. On the other hand, as shown in Figure 3B, a typical caldera-shaped PES<sup>55–60</sup> was observed for series B. There is only minor geometric distortion and hence a small energetic increase (<1 kcal/mol) from I-B (2.53, 2.63) to TS1-B (2.26, 2.56) or TS2-B (2.50, 2.30). The existence of a flat region around these three species might introduce significant dynamics effects into the reaction, making the downstream transformation of III-B a non-trivial event in the whole mechanistic scenario.<sup>61</sup> In other words, a particle coming from III-B via TS2-B might traverse this caldera-shaped area without interruption, heading for II-B. This means that although two transition states and one intermediate are located along the reaction pathway from III-B to II-B, this transformation might proceed like a concerted process to some extent.<sup>62–65</sup>

#### Direct Molecular Dynamics Simulations of the Migration Processes

To evaluate the dynamics effects in series B, we applied quasi-classical Born-Oppenheimer molecular dynamics simulations<sup>66</sup> to investigate the migration of spiroindolene III-B. First, based on TS2-B, an ensemble of initial coordinates and momenta for all the atoms of the system was sampled, which reflects how the particles traverse the nearby region of this transition state (see Figures S3 and S4 for details). Then, starting from each set of initial coordinates and momenta, a trajectory was propagated in both forward and reverse directions until either C2–C8 or C3–C8 bond was fully constructed or a total time of 2 ps was reached. Detailed analyses of 100 trajectories revealed some intriguing mechanistic information about the migration process of spiroindolene III-B from the perspective of dynamics (Figure 4). The calculated trajectories can be grouped into five categories: (1) “reactive” trajectories that proceed from III-B to II-B (44 cases), (2) “recrossing” trajectories that re-form III-B after complete breaking of C3–C8 bond (44 cases), (3) “staying” trajectories that bounce back and forth in the nearby region of I-B for over 2 ps (eight cases), (4) “reversed recrossing” trajectories that pass from II-B to the area around TS2-B and then re-form II-B (three cases), and (5) a “collapsed” trajectory that eventually leaves the caldera region (one case). Of particular interest is the observation of quite a few “reactive” trajectories (see Figures S5 and S6 and Video S1 for the details of a typical reactive trajectory). Their duration ranges from 41 to 1,993 fs, with an average value of 755 fs, which is just one order of magnitude larger than the lifetime of a

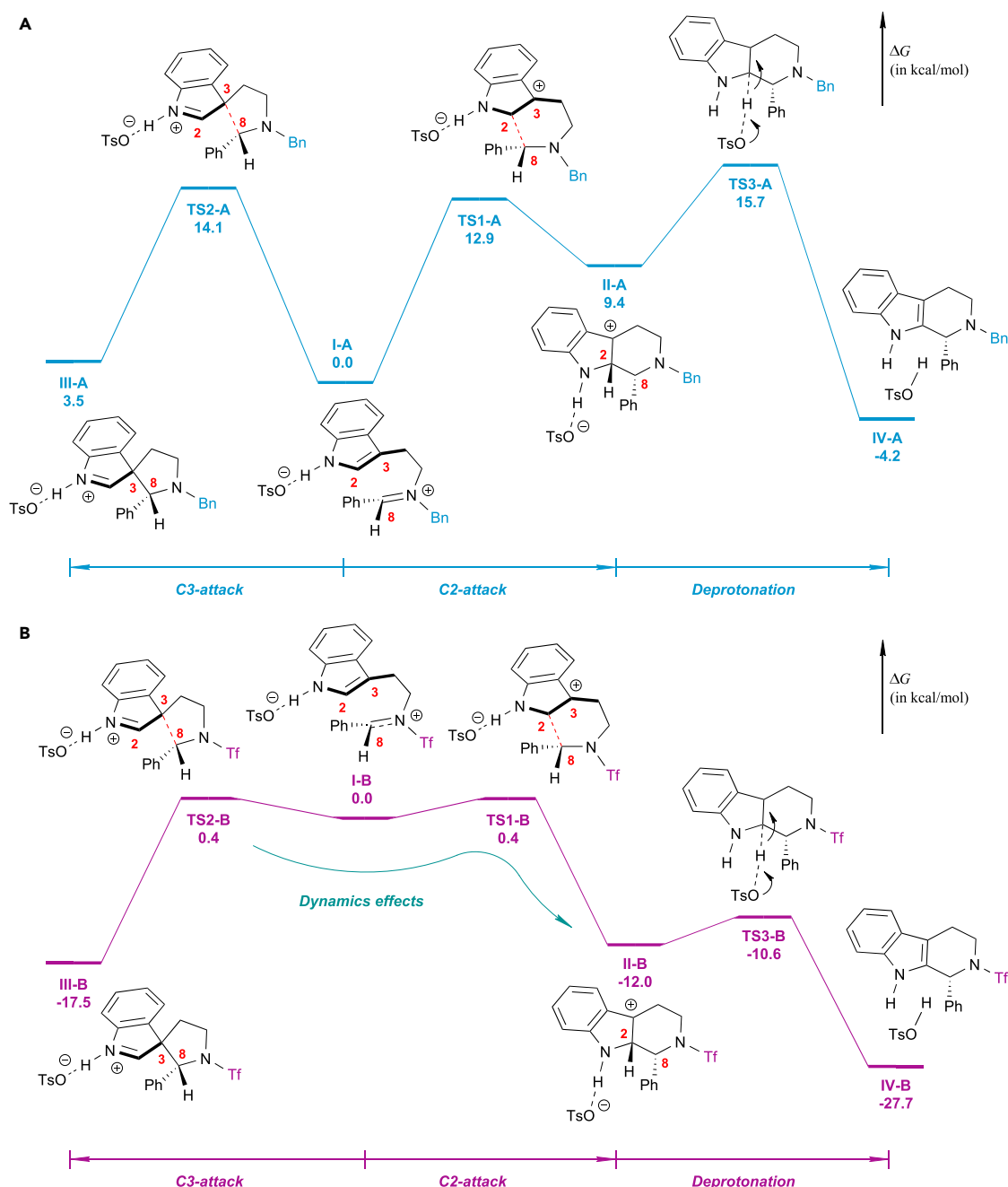


**Figure 1. The Calculated Reaction Pathways of the TsOH-Catalyzed Pictet-Spengler Reactions**

The reaction pathways with (A) N-Bn and (B) N-Tf protecting groups. Relative Gibbs free energies (in kcal/mol) were calculated at the PBE1PBE/6-311+G\*\* level of theory. The optimized structures of all stationary points can be found in Figures S1 and S2.

typical concerted transition state.<sup>67</sup> The overlay of these “reactive” trajectories (Figure 4A) perfectly matches the shape of the low-energy area in the corresponding PES (Figure 3B), which confirms a valley channel that allows direct transformation of spiroindolenine intermediate III-B to protonated tetrahydro- $\beta$ -carboline II-B. Meanwhile, the dynamics effects also contribute significantly to the stereochemistry of the reaction. In most cases, wandering of the particle in the caldera region lasts for several hundred femtoseconds no matter where a trajectory finally ends.

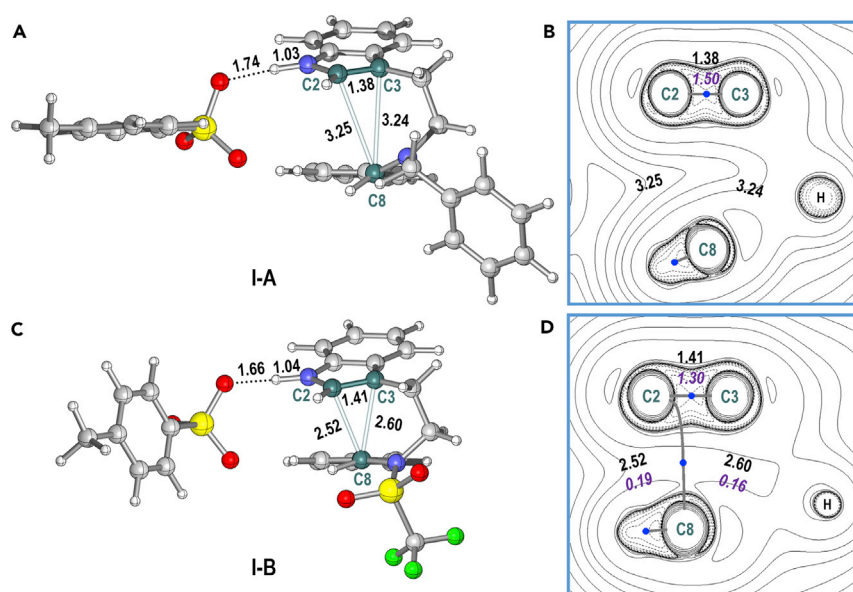


**Figure 2. The Structures of I-A and I-B**

(A and C) The optimized structures of (A) I-A and (C) I-B calculated at the PBE1PBE/6-311+G\*\* level of theory.

(B and D) The contour maps of the Laplacian of the electron density ( $\nabla^2 \rho$ ) of (B) I-A and (D) I-B in the plane defined by C2, C3, and C8. Bold values (in black) and italic values (in purple) are bond distances (in angstroms) and Wiberg bond indices, respectively, for B(C2–C3), B(C2–C8), and B(C3–C8). Blue dots indicate bond critical points. Gray lines indicate bond paths.

However, during this journey the maximum value of the average bond distance of C2–C8 and C3–C8 is roughly less than 3.5 Å, suggesting the existence of the interaction between the iminium moiety and the indole ring, which lends some stability to this “bent” conformation in which the side chain at the C3 position of the substrate is bent so that the iminium moiety is an approximation to the indole ring (Figures 4F and 4G). As a consequence, only one pro-chiral face of the iminium carbon (Si-face in this model) is oriented toward the indole ring, which guarantees the conservation of the configuration of the C8 position in the migration event. Notably, it is observed only in one case (the “collapsed” trajectory) where the distance between the iminium moiety and indole ring is elongated to over 4 Å. Hence, the racemization at the C8 position becomes possible because the “bent” conformation is completely unlocked, and, therefore, both pro-chiral faces of the free iminium carbon will be available for subsequent spiroindolization or C2 cyclization.

To make a comparison, we also performed similar direct molecular dynamics simulations for series A. Starting from initial geometries sampled on the basis of TS2-A, six trajectories were propagated for 2 ps. As expected, all the trajectories were finally trapped in the deep potential well in the nearby region of I-A and thus categorized as “staying” (see Figures S7–S9 for details). These results are in agreement with the energy profile obtained by DFT calculations (Figure 1). The attack at the C3 position of the indole ring in series A can be regarded as a simple reversible process, and there is no direct channel connecting III-A and II-A.

### Two Limiting Types of Mechanism of Pictet-Spengler Reactions

According to the results presented above, two types of mechanistic scenarios can be drawn for Pictet-Spengler reactions (Scheme 3). In both cases, the spiroindolization at the C3 position and direct cyclization at the C2 position are kinetically

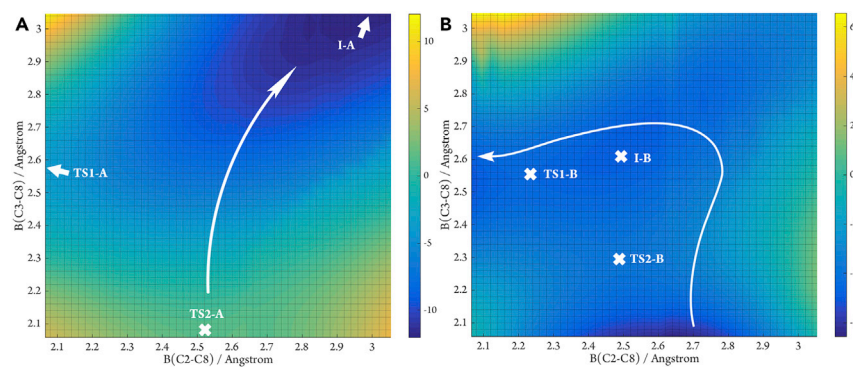


**Figure 3. The Two-Dimensional PESs of the TsOH-Catalyzed Pictet-Spengler Reactions**

The two-dimensional PESs with (A) N-Bn and (B) N-Tf protecting groups. Relative electronic energies (in kcal/mol, scaled by the colored bars) were calculated at the PBE1PBE/6-31G\*\* level of theory. The positions of selected stationary points are marked with crosses or short arrows. The schematic reaction coordinates of the migration of the corresponding spiroindolenines are shown by curved arrows.

competitive. This suggests that the formation of spiroindolenine intermediate is a common reaction pathway. However, the role of the spiroindolenine intermediate is divergent and highly depends on the shape of the PES. For the prototype substrate bearing an electron-withdrawing group (Tf) on the iminium nitrogen atom (type I), the spiroindolenine is a productive intermediate that can be transformed to protonated tetrahydro- $\beta$ -carboline, the direct precursor of the final product, via dynamics effects over the caldera-shaped PES. This corresponds to the scenario in which the migration of spiroindolenine intermediate is in operation. Moreover, in this scenario the spiroindolenine intermediate is important in terms of stereochemistry. The configuration of the iminium carbon is very likely reserved during the migration, indicating that significant chirality transfer from spiroindolenine to the final Pictet-Spengler product can be expected. On the other hand, for the prototype substrate bearing an electron-donating group (Bn) on the iminium nitrogen atom (type II), the spiroindolization process is an off-cycle equilibrium, making spiroindolenine a non-productive intermediate. There is no direct migration that connects spiroindolenine and protonated tetrahydro- $\beta$ -carboline. In addition, the configuration of the iminium carbon established in the spiroindolization process will be irrelevant to the stereochemistry of the final product. Notably, in the type II scenario the final deprotonation is the rate-determining step, whereas in the type I scenario, it is not.

### Experimental Verifications

To test the aforementioned theoretical predictions experimentally, we prepared spiroindolines **1a** (N-Ts) and **1b** (N-Bn) in enantioenriched form and subjected them to a sequential oxidation and migration reaction (*Scheme 4*). With manganese dioxide ( $MnO_2$ ) or iodosobenzene ( $PhIO$ ) as the oxidant, the secondary amine moieties of **1a** and **1b** could be converted to imines. The *in-situ*-formed spiroindolenines underwent iminium migration in the presence of racemic phosphoric acid (rac-PA), delivering their corresponding tetrahydro- $\beta$ -carbolines **2a** and **2b** in moderate yields. Notably, compound **2a** was afforded in 95% enantiomeric excess (ee), and **2b** was afforded in completely racemic form. These results serve as solid evidence supporting the two limiting mechanistic scenarios proposed in the previous section.

### Applications in Selected Known Pictet-Spengler Reactions

Our next aim was to investigate how the two limiting mechanistic scenarios can be applied in more realistic situations. In this regard, seven representative examples

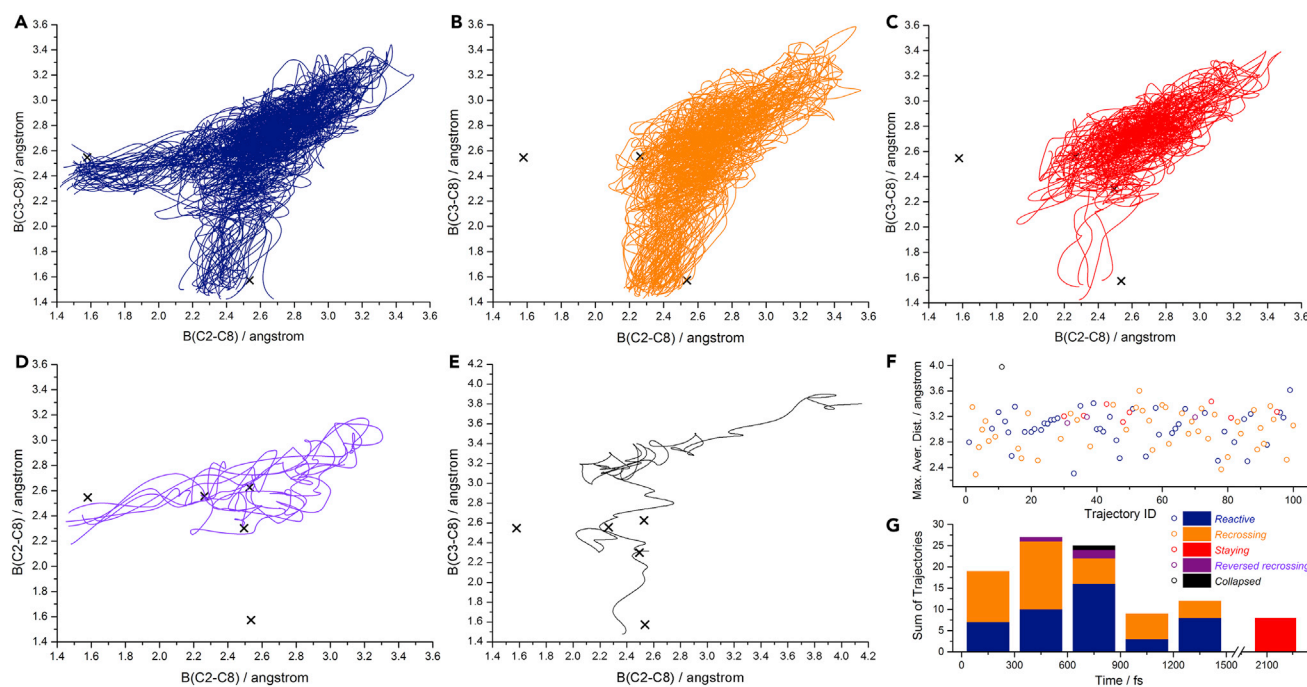


**Figure 4. The Results of BOMD Calculations**

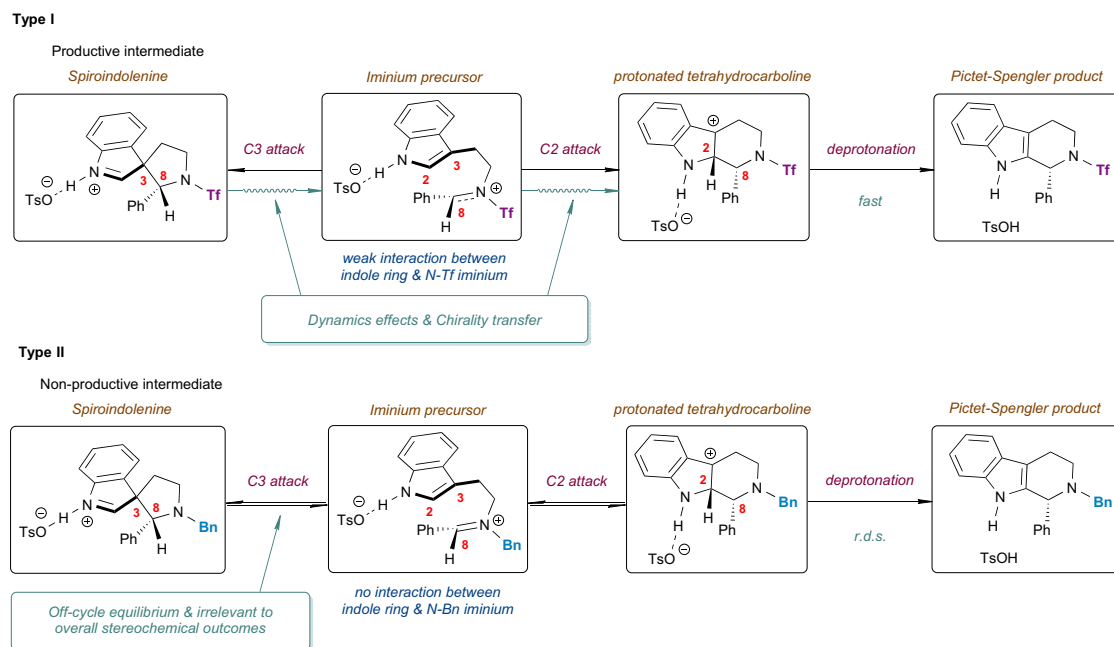
(A–E) The overlays of the plots of “reactive” (A, blue), “recrossing” (B, orange), “staying” (C, red), “reversed recrossing” (D, purple), and “collapsed” (E, black) trajectories of series B with respect to the distances of C2–C8 and C3–C8 bonds. Black crosses show the stationary points (I–B (2.53, 2.63), TS1–B (2.26, 2.56), II–B (1.58, 2.55), TS2–B (2.50, 2.30), and III–B (2.54, 1.57)) of the PES.

(F) Summary of maximum average distance of C2–C8 and C3–C8 bonds during a trajectory.

(G) Distribution of the duration of each trajectory in the time scales of 0–300, 300–600, 600–900, 900–1,200, 1,200–2,000, and >2,000 fs.

of known catalytic asymmetric Pictet-Spengler reactions<sup>68–74</sup> were considered (**Scheme 5**). These reactions were catalyzed by either a chiral phosphoric acid or a chiral thiourea. A wide range of iminium precursors with diverse steric and electronic properties of the side chains were covered. The key intermediates and transition states of each system (series C–I) with a truncated catalyst were optimized at the PBE1PBE/6-311+G\*\* level of theory (see **Table S3** for details). Interestingly, the energy profiles of these “real” Pictet-Spengler reactions varied significantly from each other. To accomplish unified understandings of the mechanism of Pictet-Spengler reactions, we developed a mechanistic diagram on the basis of the two parameters ( $d$  and  $h$ ) that we employed to characterize the shape of the PES of the reaction (**Figure 5**). All the series studied herein can be scattered into this diagram according to their own  $d$  and  $h$  values. Each series is represented as either a black cross or a red circle depending on whether the deprotonation is the rate-determining step or not.

As discussed in previous sections,  $d$  and  $h$  values are two key parameters that characterize the shape of the PES of a Pictet-Spengler reaction. A smaller  $d$  value indicates a larger possibility that a spiroindolenine intermediate can be formed in the reaction. On the other hand, a smaller  $h$  value indicates a more typical caldera-shaped PES, and hence larger possibility that a productive migration of spiroindole-nine intermediate is involved via dynamics effects. In our mechanistic diagram, the two prototype reactions, series A (13.5, 1.2) and B (0.4, 0.0), are located in the right side and the lower-left corner, respectively, as two references. The detailed knowledge about these two series obtained in this study will help interpretation of the mechanistic aspects of other enantioselective Pictet-Spengler reactions. In cases

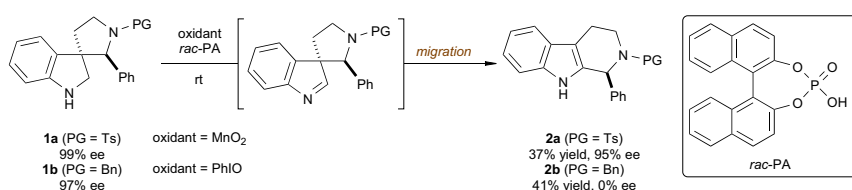


**Scheme 3. Two Limiting Types of Mechanism of Pictet-Spengler Reactions**

where a relatively small  $d$  value is observed—series C (2.8, 1.3), D (13.1, 0.8), and I (6.8, 1.7)—the spiroindolenine intermediates might be formed in a non-negligible proportion.<sup>75</sup> Among these cases, series D resembles series A the most in that the spiroindolenine serves as non-productive intermediate. Although with a relatively less typical caldera-shaped PES, we believe that series C behaves like series B to some extent. The spiroindolenine intermediates formed in this reaction can migrate without significant interruption. The stereochemistry established during the spiroindolization process will contribute to that of the final Pictet-Spengler product. With a medium-level  $h$  value, series I resides in the somewhat borderline region of the mechanistic spectrum. In this case, we believe that both types of limiting mechanisms of Pictet-Spengler reactions might be in operation at the same time. For the cases with a larger  $d$  value such as series E (4.3, 3.4), F (5.4, 3.7), G (10.0, 2.3), and H (9.8, 3.5), a much higher energetic barrier is required to be overcome for the spiroindolization than that for the direct C2 cyclization. Therefore, the spiroindolization becomes a minor process in the whole reaction, and the downstream transformation of spiroindolenine species is of less importance. In series A and F, the final deprotonation was identified as the rate-determining step. Thus, the stereochemistry of the reaction might be irrelevant to both spiroindolization and C2 cyclization processes.<sup>41</sup> This mechanistic spectrum shows that, although the structural perturbation of substrate and the switch of catalyst will alter the profile of Pictet-Spengler reactions significantly, a quick but insightful interpretation of the mechanism of a given Pictet-Spengler reaction can be drawn on the basis of two simple parameters ( $d$  and  $h$ ) in energetics.

## Conclusion

In this study, we performed detailed computational studies on the mechanism of Pictet-Spengler reactions. Combined DFT calculations and direct molecular dynamics simulations were carried out on two prototype reactions, from which two types of limiting mechanistic scenarios have been proposed. The divergent roles played by spiroindolenines, key intermediates commonly proposed in previous



**Scheme 4. The Experimental Verifications of the Mechanistic Proposals**

mechanisms, have been demonstrated. These theoretical predictions were supported by experimental investigations. In addition, the current work serves as a vivid example showing the possibility that the stereochemical outcomes of a synthetically useful reaction might be complexed by dynamics effects, a term beyond traditional TST.<sup>76,77</sup> On the basis of the two limiting scenarios, a comprehensive mechanistic spectrum was developed and applied to several representative examples of known catalytic asymmetric Pictet-Spengler reactions. We believe that these results can be utilized as a practical guide in exploring novel reactivity of spiroindolenine species and related chemistry.

## EXPERIMENTAL PROCEDURES

### Computational Part

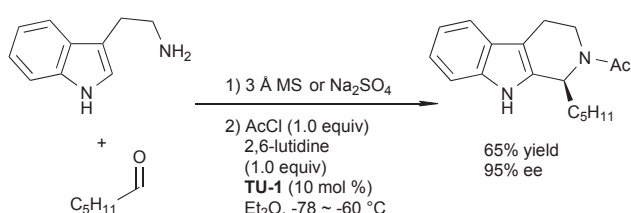
All the calculations in this study were performed with the Gaussian09 package.<sup>78</sup> During the exploration of the reaction profile, the DFT method was employed with the PBE1PBE functional. The standard 6-311+G\*\* basis sets were applied for all atoms. Optimizations were conducted without any constraint according to the implicit solvation model (SMD) in THF ( $\epsilon = 7.4257$ ). Frequency analyses were carried out to confirm each structure being a minimum (no imaginary frequency) or a transition state (only one imaginary frequency). Ultrafine grid was specified for numerical integrations. Benchmark calculations with PBE1PPBE, M06-2X,  $\omega$ B97XD, and B3LYP-D3(BJ) functionals were performed with 6-31G\*\* or 6-311+G\*\* basis sets and the same solvation model. Two-dimensional relaxed PES scans were carried out at the PBE1PBE/6-31G\*\* level of theory. Quasi-classical Born-Oppenheimer molecular dynamics simulations were performed with the “BOMD” keyword implemented in Gaussian09 package. The initial coordinates and momenta of all the trajectories were generated from the normal mode sampling (at 300 K) from the transition state TS2-B or TS2-A optimized at the PBE1PBE/6-31G\*\* level of theory. From each set of initial coordinates and momenta, a trajectory was propagated with the classical equations of motion with energies and forces computed with PBE1PBE/6-31G\*\* in THF (SMD). Trajectory propagation was performed in both forward and reverse directions until either C2–C8 or C3–C8 bond was fully constructed or a total time of 2 ps was reached. AIM topological analysis and Wiberg bond index analysis were performed with Multiwfn.<sup>79</sup> All calculated structures were visualized with CYLview<sup>80</sup> or VMD.<sup>81</sup>

### Experimental Part

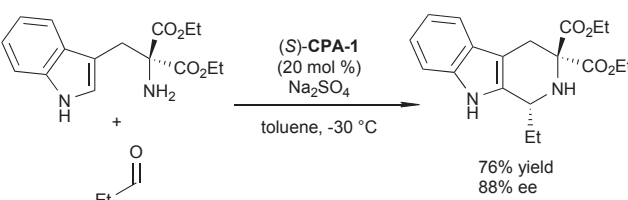
#### The Procedure of Sequential Oxidation and Migration Reaction of 1a

Anhydrous dichloroethane (2 mL) and MnO<sub>2</sub> (284.0 mg, 3 mmol, 92% w/w) were added to a mixture of 1a (41.0 mg, 0.1 mmol, 99% ee), rac-PA (7.0 mg, 0.02 mmol), and 3 Å MS (100 mg) under argon. The reaction mixture was stirred at 25°C and monitored by thin-layer chromatography (TLC). Upon its completion, the reaction was quenched with saturated NaHCO<sub>3</sub> and extracted with dichloromethane ( $\times 3$ ). The combined organic layer was washed with brine, dried over Na<sub>2</sub>SO<sub>4</sub>, and filtrated. After the solvent was removed under reduced pressure, the residue

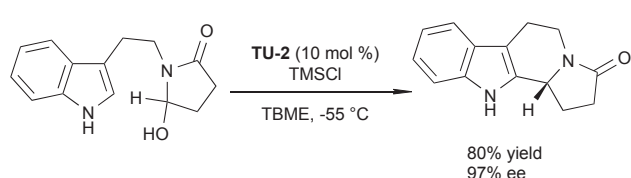
Series C<sup>68</sup>



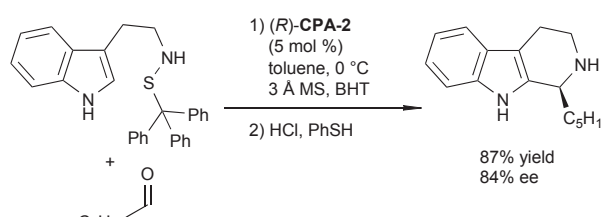
Series D<sup>69</sup>



Series E<sup>70</sup>

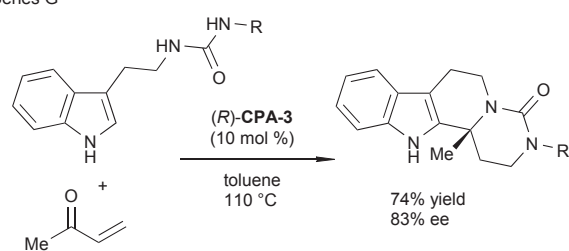


Series F<sup>71</sup>



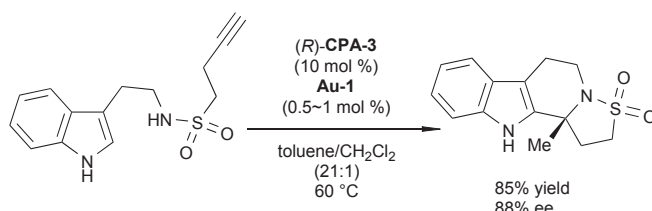
BHT = 3,5-(*t*Bu)<sub>2</sub>-4-hydroxytoluene

Series G<sup>72</sup>

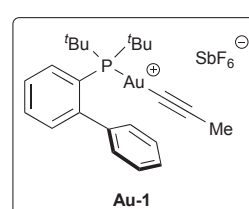
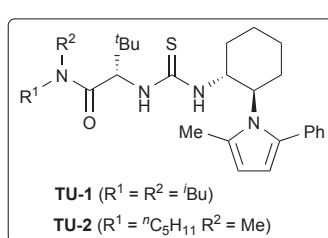
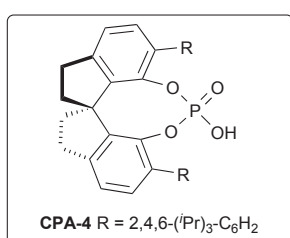
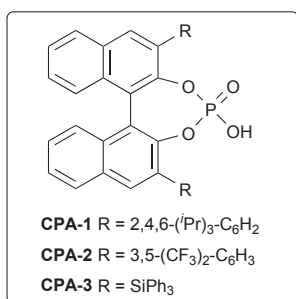
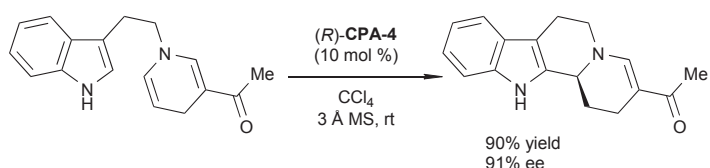


R = *p*-FC<sub>6</sub>H<sub>4</sub>

Series H<sup>73</sup>



Series I<sup>74</sup>



Scheme 5. Representative Examples of Known Catalytic Asymmetric Pictet-Spengler Reactions Considered in This Study

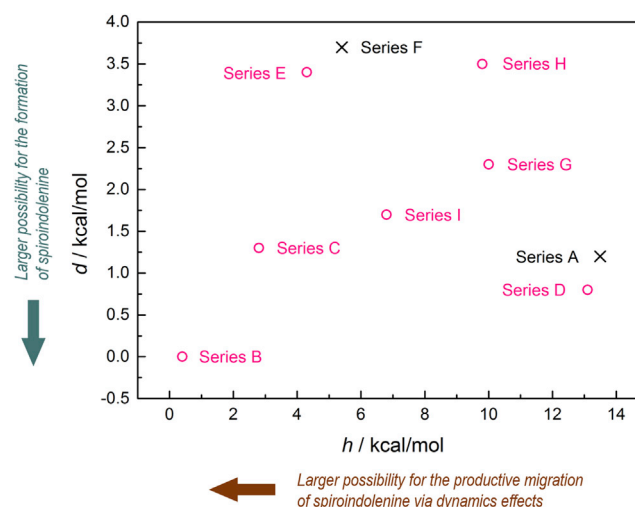


**Figure 5. The Two-Dimensional Mechanistic Spectrum of Pictet-Spengler Reactions**

The spectrum was established on the basis of parameters  $d$  (the energy difference between transition states of spiroindolization and C2 cyclization processes) and  $h$  (the average barrier height of spiroindolization and C2 cyclization processes) values. Each series is represented by a black cross (deprotonation is the rate-determining step) or a red circle (deprotonation is not the rate-determining step).

was purified by preparative TLC (ethyl acetate/petroleum ether = 1/4) to afford **2a** (15.0 mg, 37% yield, 95% ee).

#### *The Procedure of Sequential Oxidation and Migration Reaction of **1b***

Anhydrous dichloroethane (4 mL) and PhIO (53.0 mg, 0.24 mmol) were added to a mixture of **1b** (68.0 mg, 0.2 mmol, 97% ee), rac-PA (7.0 mg, 0.02 mmol), and 3 Å MS (200 mg) under argon. The reaction mixture was stirred at 25°C and monitored by TLC. Upon its completion, the reaction was quenched with saturated NaHCO<sub>3</sub> and extracted with dichloromethane ( $\times 3$ ). The combined organic layer was washed with brine, dried over Na<sub>2</sub>SO<sub>4</sub>, and filtrated. After the solvent was removed under reduced pressure, the residue was purified by preparative TLC (ethyl acetate/petroleum ether = 1/9) to afford **2b** (26.0 mg, 41% yield, 0% ee).

More detailed information can be found in the *Supplemental Information* (Scheme S1, Figures S10–S25, and associated text).

#### **DATA AND SOFTWARE AVAILABILITY**

The structure of compound **4** (reported in the *Supplemental Information*) has been deposited in the Cambridge Crystallographic Data Centre under accession number CCDC: 1811798.

#### **SUPPLEMENTAL INFORMATION**

Supplemental Information includes Supplemental Experimental Procedures, 25 figures, 1 scheme, 3 tables, 1 video, and 1 data file and can be found with this article online at <https://doi.org/10.1016/j.chempr.2018.06.006>.

#### **ACKNOWLEDGMENTS**

We thank the National Key R&D Program of China (2016YFA0202900), the National Basic Research Program of China (973 Program 2015CB856600), the National

Natural Science Foundation of China (21332009 and 21772219), the Science and Technology Commission of Shanghai Municipality (16XD1404300 and 18QA1404900), and the Strategic Priority Research Program (XDB20000000), Key Research Program of Frontier Sciences (QYZDYSSWLSH012), and Youth Innovation Promotion Association (2017302) of the Chinese Academy of Sciences for generous financial support.

## AUTHOR CONTRIBUTIONS

C.Z. contributed the concepts and ideas, performed the computations, analyzed data, and drafted and revised the manuscript. Z.-L.X. performed the experimental studies. C.Z., Z.-L.X., and S.-L.Y. commented on the results. S.-L.Y. conceived the project and served as the principal investigator.

## DECLARATION OF INTERESTS

The authors declare no competing interests.

Received: April 1, 2018

Revised: May 9, 2018

Accepted: June 12, 2018

Published: July 12, 2018

## REFERENCES AND NOTES

- Walden, D.M., Ogba, O.M., Johnston, R.C., and Cheong, P.H.-Y. (2016). Computational insights into the central role of nonbonding interactions in modern covalent organocatalysis. *Acc. Chem. Res.* **49**, 1279–1291.
- Sigman, M.S., Harper, K.C., Bess, E.N., and Milo, A. (2016). The development of multidimensional analysis tools for asymmetric catalysis and beyond. *Acc. Chem. Res.* **49**, 1292–1301.
- Zhang, X., Chung, L.W., and Wu, Y.-D. (2016). New mechanistic insights on the selectivity of transition-metal-catalyzed organic reactions: The role of computational chemistry. *Acc. Chem. Res.* **49**, 1302–1310.
- Sperger, T., Sanhueza, I.A., and Schoenebeck, F. (2016). Computation and experiment: A powerful combination to understand and predict reactivities. *Acc. Chem. Res.* **49**, 1311–1319.
- Ess, D.H., Wheeler, S.E., Ifae, R.G., Xu, L., Çelebi-Ölçüm, N., and Houk, K.N. (2008). Bifurcations on potential energy surfaces of organic reactions. *Angew. Chem. Int. Ed.* **47**, 7592–7601.
- Lourderaj, U., Park, K., and Hase, W.L. (2008). Classical trajectory simulations of post-transition state dynamics. *Int. Rev. Phys. Chem.* **27**, 361–403.
- Rehbein, J., and Carpenter, B.K. (2011). Do we fully understand what controls chemical selectivity? *Phys. Chem. Chem. Phys.* **13**, 20906–20922.
- Bachrach, S.M. (2014). Chapter 8. Organic reaction dynamics. In *Computational Organic Chemistry*, Second Edition (Wiley).
- Hare, S.R., and Tantillo, D.J. (2016). Dynamic behavior of rearranging carbocations—implications for terpene biosynthesis. *Beilstein J. Org. Chem.* **12**, 377–390.
- Pratihar, S., Ma, X., Homayoon, Z., Barnes, G.L., and Hase, W.L. (2017). Direct chemical dynamics simulations. *J. Am. Chem. Soc.* **139**, 3570–3590.
- Yang, Z., and Houk, K.N. (2018). The dynamics of chemical reactions: atomistic visualizations of organic reactions, and homage to von't Hoff. *Chem. Eur. J.* **24**, 3916–3924.
- López, J.G., Vayner, G., Lourderaj, U., Addepalli, S.V., Kato, S., deJong, W.A., Windus, T.L., and Hase, W.L. (2007). A direct dynamics trajectory study of F- + CH<sub>3</sub>OOH reactive collisions reveals a major non-IRC reaction path. *J. Am. Chem. Soc.* **129**, 9976–9985.
- Hong, Y.J., and Tantillo, D.J. (2009). A potential energy surface bifurcation in terpene biosynthesis. *Nat. Chem.* **1**, 384–389.
- Oyola, Y., and Singleton, D.A. (2009). Dynamics and the failure of transition state theory in alkene hydroboration. *J. Am. Chem. Soc.* **131**, 3130–3131.
- Hansen, J.H., Gregg, T.M., Ovalles, S.R., Lian, Y., Autschbach, J., and Davies, H.M.L. (2011). On the mechanism and selectivity of the combined C-H activation/Cope rearrangement. *J. Am. Chem. Soc.* **133**, 5076–5085.
- Siebert, M.R., Zhang, J., Addepalli, S.V., Tantillo, D.J., and Hase, W.L. (2011). The need for enzymatic steering in abietic acid biosynthesis: gas-phase chemical dynamics simulations of carbocation rearrangements on a bifurcating potential energy surface. *J. Am. Chem. Soc.* **133**, 8335–8343.
- Biswas, B., Collins, S.C., and Singleton, D.A. (2014). Dynamics and a unified understanding of competitive [2,3]- and [1,2]-sigmatropic rearrangements based on a study of ammonium ylides. *J. Am. Chem. Soc.* **136**, 3740–3743.
- Biswas, B., Bercovici, D.A., Yang, Z., Al-Bataineh, N., Srinivasan, R., Dhakal, R.C., Houk, K.N., and Brewer, M. (2015). Mechanism and dynamics of intramolecular C-H insertion reactions of 1-aza-2-azoniaallene salts. *J. Am. Chem. Soc.* **137**, 9100–9107.
- Biswas, B., and Singleton, D.A. (2015). Controlling selectivity by controlling the path of trajectories. *J. Am. Chem. Soc.* **137**, 14244–14247.
- Patel, A., Chen, Z., Yang, Z., Gutiérrez, O., Liu, H.-w., Houk, K.N., and Singleton, D.A. (2016). Dynamically complex [6+4] and [4+2] cycloadditions in the biosynthesis of spinosyn A. *J. Am. Chem. Soc.* **138**, 3631–3634.
- Yang, Z., Yu, P., and Houk, K.N. (2016). Molecular dynamics of dimethyldioxirane C-H oxidation. *J. Am. Chem. Soc.* **138**, 4237–4242.
- Nieves-Quinones, Y., and Singleton, D.A. (2016). Dynamics and the regiochemistry of nitration of toluene. *J. Am. Chem. Soc.* **138**, 15167–15176.
- McFadden, T.R., Fang, C., Geib, S.J., Merling, E., Liu, P., and Curran, D.P. (2017). Synthesis of boranes by double hydroboration reactions of N-heterocyclic carbene boranes and dimethyl acetylenedicarboxylate. *J. Am. Chem. Soc.* **139**, 1726–1729.

25. Aziz, H.R., and Singleton, D.A. (2017). Concert along the edge: dynamics and the nature of the border between general and specific acid-base catalysis. *J. Am. Chem. Soc.* 139, 5965–5972.
26. Grayson, M.N., Yang, Z., and Houk, K.N. (2017). Chronology of CH $\cdots$ O hydrogen bonding from molecular dynamics studies of the phosphoric acid-catalyzed allylboration of benzaldehyde. *J. Am. Chem. Soc.* 139, 7717–7720.
27. Yu, P., Chen, T.Q., Yang, Z., He, C.Q., Patel, A., Lam, Y.-h., Liu, C.-Y., and Houk, K.N. (2017). Mechanisms and origins of periselectivity of the ambimodal [6+4] cycloadditions of tropone to dimethylfulvene. *J. Am. Chem. Soc.* 139, 8251–8258.
28. Hare, S.R., and Tantillo, D.J. (2017). Cryptic post-transition state bifurcations that reduce the efficiency of lactone-forming Rh-carbenoid C-H insertions. *Chem. Sci.* 8, 1442–1449.
29. Yang, Z., Yang, S., Yu, P., Li, Y., Doubleday, C., Park, J., Patel, A., Jeon, B.-s., Russell, W.K., Liu, H.-w., et al. (2018). Influence of water and enzyme SpnF on the dynamics and energetics of the ambimodal [6+4]/[4+2] cycloaddition. *Proc. Natl. Acad. Sci. USA* 115, E848–E855.
30. Cox, E.D., and Cook, J.M. (1995). The Pictet-Spengler condensation: a new direction for an old reaction. *Chem. Rev.* 95, 1797–1842.
31. Royer, J., Bonin, M., and Micouin, L. (2004). Chiral heterocycles by iminium ion cyclization. *Chem. Rev.* 104, 2311–2352.
32. Lorenz, M., Van Linn, M.L., and Cook, J.M. (2010). The asymmetric Pictet-Spengler reaction. *Curr. Org. Synth.* 7, 189–223.
33. Stöckigt, J., Antonchick, A.P., Wu, F., and Waldmann, H. (2011). The Pictet-Spengler reaction in nature and in organic chemistry. *Angew. Chem. Int. Ed.* 50, 8538–8564.
34. Kundu, B., Agarwal, P.K., Sharma, S.K., Sawant, D., Mandadapu, A.K., Saifuddin, M., and Gupta, S. (2012). Pictet-Spengler reaction revisited: engineering of tethered biheterocycles into annulated polyheterocycles. *Curr. Org. Synth.* 9, 357–376.
35. Jackson, A.H., and Smith, A.E. (1968). Electrophilic substitution in indoles—II: the formation of 3,3-spirocyclic indole derivatives from tryptamines and their rearrangement to  $\beta$ -carbolines. *Tetrahedron* 24, 403–413.
36. Bailey, P.D. (1987). On the stereochemistry of the Pictet-Spengler reaction. *Tetrahedron Lett.* 28, 5181–5184.
37. Bailey, P.D. (1987). Direct proof of the involvement of a spiro intermediate in the Pictet-Spengler reaction. *J. Chem. Res. S.*, 202–203.
38. Kowalski, P., and Mokrosz, J.L. (1997). Structure and spectral properties of  $\beta$ -carbolines. Part 9. New arguments against direct rearrangement of the spiroindoline intermediate into  $\beta$ -carboline system in the Pictet-Spengler cyclization. An MNDO approach. *Bull. Soc. Chim. Belg.* 106, 147–149.
39. Maresh, J.J., Giddings, L.-A., Friedrich, A., Loris, E.A., Panjikar, S., Trout, B.L., Stöckigt, J., Peters, B., and O'Connor, S.E. (2008).
40. Overoerde, L.M., Grayson, M.N., Luo, Y., and Goodman, J.M. (2015). Mechanistic insights into a BINOL-derived phosphoric acid-catalyzed asymmetric Pictet-Spengler reaction. *J. Org. Chem.* 80, 2634–2640.
41. Klausen, R.S., Kennedy, C.R., Hyde, A.M., and Jacobsen, E.N. (2017). Chiral thioureas promote enantioselective Pictet-Spengler cyclization by stabilizing every intermediate and transition state in the carboxylic acid-catalyzed reaction. *J. Am. Chem. Soc.* 139, 12299–12309.
42. Gobé, V., Gandon, V., and Guinchard, X. (2018). Reactions involving tryptamines and  $\delta$ -allyl aldehydes: competition between Pictet-Spengler reaction and cyclization to 1-aminotetralins. *Adv. Synth. Catal.* 360, 1280–1288.
43. James, M.J., O'Brien, P., Taylor, R.J.K., and Unsworth, W.P. (2016). Synthesis of spirocyclic indolenines. *Chem. Eur. J.* 22, 2856–2881.
44. Zhuo, C.-X., Zheng, C., and You, S.-L. (2014). Transition-metal-catalyzed asymmetric allylic dearomatization reactions. *Acc. Chem. Res.* 47, 2558–2573.
45. Zheng, C., and You, S.-L. (2016). Catalytic asymmetric dearomatization by transition-metal catalysis: a method for transformations of aromatic compounds. *Chem.* 1, 830–857.
46. Wu, Q.-F., He, H., Liu, W.-B., and You, S.-L. (2010). Enantioselective construction of spiroindolenines by Ir-catalyzed allylic alkylation reactions. *J. Am. Chem. Soc.* 132, 11418–11419.
47. Wu, Q.-F., Zheng, C., and You, S.-L. (2012). Enantioselective synthesis of spiro cyclopentane-1,3'-indoles and 2,3,4,9-tetrahydro-1H-carbazoles by iridium-catalyzed allylic dearomatization and stereospecific migration. *Angew. Chem. Int. Ed.* 51, 1680–1683.
48. Zhuo, C.-X., Wu, Q.-F., Zhao, Q., Xu, Q.-L., and You, S.-L. (2013). Enantioselective functionalization of indoles and pyrroles via an *in situ* formed spiro intermediate. *J. Am. Chem. Soc.* 135, 8169–8172.
49. Zhuo, C.-X., Zhou, Y., Cheng, Q., Huang, L., and You, S.-L. (2015). Enantioselective construction of spiroindolines with three contiguous stereogenic centers and chiral tryptamine derivatives via reactive spiroindoline intermediates. *Angew. Chem. Int. Ed.* 54, 14146–14149.
50. Wu, Q.-F., Zheng, C., Zhuo, C.-X., and You, S.-L. (2016). Highly efficient synthesis and stereoselective migration reactions of chiral five-membered aza-spiroindolenines: scope and mechanistic understanding. *Chem. Sci.* 7, 4453–4459.
51. Wang, Y., Zheng, C., and You, S.-L. (2017). Ir-catalyzed asymmetric allylic dearomatization via a desymmetrization strategy. *Angew. Chem. Int. Ed.* 56, 15093–15097.
52. Zheng, C., Wu, Q.-F., and You, S.-L. (2013). A combined theoretical and experimental investigation into the highly stereoselective migration of spiroindolenines. *J. Org. Chem.* 78, 4357–4365.
53. Bader, R.F.W. (1985). Atoms in molecules. *Acc. Chem. Res.* 18, 9–15.
54. Wiberg, K.B. (1968). Application of the Pople-Santry-Segal CNDO method to the cyclopropylcarbinyl and cyclobutyl cation and to bicyclobutane. *Tetrahedron* 24, 1083–1096.
55. Carpenter, B.K. (1996). Bimodal distribution of lifetimes for an intermediate from a quasiclassical dynamics simulation. *J. Am. Chem. Soc.* 118, 10329–10330.
56. Reyes, M.B., Lobkovsky, E.B., and Carpenter, B.K. (2002). Interplay of the orbital symmetry and nonstatistical dynamics in the thermal rearrangements of bicyclo[n.1.0]polyenes. *J. Am. Chem. Soc.* 124, 641–651.
57. Doering, W.V.E., Cheng, X., Lee, K., and Lin, Z. (2002). Fate of the intermediate diradicals in the caldera: stereochemistry of thermal stereoremutations, (2+2) cycloreversions, and (2+4) ring-enlargements of *cis*- and *trans*-1-cyano-2-(E and Z)-propenyl-*cis*-3,4-dideuteriocyclobutanes. *J. Am. Chem. Soc.* 124, 11642–11652.
58. Doubleday, C., Suhada, C.P., and Houk, K.N. (2006). Dynamics of the degenerate rearrangement of bicyclo[3.1.0]hex-2-ene. *J. Am. Chem. Soc.* 128, 90–94.
59. Chen, Z., Nieves-Quinones, Y., Waas, J.R., and Singleton, D.A. (2014). Isotope effects, dynamic matching, and solvent dynamics in a Wittig reaction. Betaines as bypassed intermediates. *J. Am. Chem. Soc.* 136, 13122–13125.
60. Törk, L., Jiménez-Osés, G., Doubleday, C., Liu, F., and Houk, K.N. (2015). Molecular dynamics of the Diels-Alder reactions of tetrazines with alkenes and N<sub>2</sub> extrusions from adducts. *J. Am. Chem. Soc.* 137, 4749–4758.
61. Because of the existence of the caldera-shaped area of the PES in series B, the regioselectivity in the first step (spiroindolization versus C2 cyclization) might not be entirely determined by the energetic difference between TS1-B and TS2-B but also complicated by some possible dynamics effects.
62. Siebert, M.R., and Tantillo, D.J. (2007). Transition-state complexation in palladium-promoted [3,3] sigmatropic shifts. *J. Am. Chem. Soc.* 129, 8686–8687.
63. Gilmore, K., Manoharan, M., Wu, J.I.-C., Schleyer, P.v.R., and Alabugin, I.V. (2012). Aromatic transition states in nonpericyclic reactions: anionic 5-endo cyclizations are aborted sigmatropic shifts. *J. Am. Chem. Soc.* 134, 10584–10594.
64. Vidhani, D.V., Krafft, M.E., and Alabugin, I.V. (2016). Gold(I)-catalyzed allyl Cope rearrangement: evolution from asynchronicity to trappable intermediates assisted by stereoelectronic switching. *J. Am. Chem. Soc.* 138, 2769–2779.
65. dos Passos Gomes, G., and Alabugin, I.V. (2017). Drawing catalytic power from charge separation: stereoelectronic and zwitterionic assistance in the Au(I)-catalyzed Bergman cyclization. *J. Am. Chem. Soc.* 139, 3406–3416.

66. Bolton, K., Hase, W.L., and Peslherbe, G.H. (1998). Direct dynamics simulations of reactive systems. In *Modern Methods for Multidimensional Dynamics Computation in Chemistry*, D.L. Thompson, ed. (World Scientific), pp. 143–189.
67. Black, K., Liu, P., Xu, L., Doubleday, C., and Houk, K.N. (2012). Dynamics, transition states, and timing of bond formation in Diels-Alder reactions. *Proc. Natl. Acad. Sci. USA* **109**, 12860–12865.
68. Taylor, M.S., and Jacobsen, E.N. (2004). Highly enantioselective catalytic acyl-Pictet-Spengler reactions. *J. Am. Chem. Soc.* **126**, 10558–10559.
69. Seayad, J., Seayad, A.M., and List, B. (2006). Catalytic asymmetric Pictet-Spengler reaction. *J. Am. Chem. Soc.* **128**, 1086–1087.
70. Raheem, I.T., Thiara, P.S., Peterson, E.A., and Jacobsen, E.N. (2007). Enantioselective Pictet-Spengler-type cyclizations of hydroxylactams: H-bond donor catalysis by anion binding. *J. Am. Chem. Soc.* **129**, 13404–13405.
71. Wanner, M.J., van der Haas, R.N.S., de Cuba, K.R., van Maarseveen, J.H., and Hiemstra, H. (2007). Catalytic asymmetric Pictet-Spengler reactions via sulfonyliminium ions. *Angew. Chem. Int. Ed.* **46**, 7485–7487.
72. Aillaud, I., Barber, D.M., Thompson, A.L., and Dixon, D.J. (2013). Enantioselective Michael addition/iminium ion cyclization cascades of tryptamine-derived ureas. *Org. Lett.* **15**, 2946–2949.
73. Gregory, A.W., Jakubec, P., Turner, P., and Dixon, D.J. (2013). Gold and BINOL-phosphoric acid catalyzed enantioselective hydroamination/*N*-sulfonyliminium cyclization cascade. *Org. Lett.* **15**, 4330–4333.
74. Wang, S.-G., Xia, Z.-L., Xu, R.-Q., Liu, X.-J., Zheng, C., and You, S.-L. (2017). Construction of chiral tetrahydro- $\beta$ -carbolines: asymmetric Pictet-Spengler reaction of indolyl dihydropyridines. *Angew. Chem. Int. Ed.* **56**, 7440–7443.
75. Chambers, S.J., Coulthard, G., Unsworth, W.P., O'Brien, P., and Taylor, R.J.K. (2016). From heteroaromatic acids and imines to azaspirocycles: stereoselective synthesis and 3D shape analysis. *Chem. Eur. J.* **22**, 6496–6500.
76. Noey, E.L., Wang, X., and Houk, K.N. (2011). Selective gold(II)-catalyzed formation of tetracyclic indolines: a single transition structure and bifurcations lead to multiple products. *J. Org. Chem.* **76**, 3477–3483.
77. Zhang, L., Wang, Y., Yao, Z.-J., Wang, S., and Yu, Z.-X. (2015). Kinetic or dynamic control on a bifurcating potential energy surface? An experimental and DFT study of gold-catalyzed ring expansion and spirocyclization of 2-propargyl- $\beta$ -tetrahydrocarbolines. *J. Am. Chem. Soc.* **137**, 13290–13300.
78. Frisch, M.J., Trucks, G.W., Schlegel, H.B., Scuseria, G.E., Robb, M.A., Cheeseman, J.R., Scalmani, G., Barone, V., Petersson, G.A., Nakatsuji, H., et al. (2013). Gaussian09, Revision D.01 (Gaussian, Inc.).
79. Lu, T., and Chen, F. (2012). Multiwfn: a multifunctional wavefunction analyzer. *J. Comput. Chem.* **33**, 580–592.
80. Legault, C.Y. (2009). CYLView, 1.0b (Université de Sherbrooke). <http://www.cylview.org>.
81. Humphrey, W., Dalke, A., and Schulter, K. (1996). VMD: visual molecular dynamics. *J. Mol. Graph.* **14**, 33–38.